Supporting Information

Erdel and Rippe 10.1073/pnas.1209579109

SI Text

Scale-Dependent Behavior of Reaction-Diffusion Processes. Simple diffusion processes can be studied on different length and time scales because the diffusion coefficient is scale-independent for length scales significantly larger than the mean free path and for time scales well above the inverse collision rate. However, this is different for a reaction-diffusion process that exhibits different scale-dependent properties. For the theoretical description given below, it is instructive to consider a reaction-diffusion process as a pseudofirst-order reaction, in which particles exchange between a free state (F) and an immobile complex (C). In biological systems, this scenario reflects the binding of a mobile factor to an essentially immobile substrate with an excess of potential binding sites, such as chromatin in the cell nucleus or the cytoskeleton in the cytosol. The probability to find particles in the free or the bound state depends on the kinetic on and off rates for binding, k_{on} and k_{off}, and obeys the following differential equations:

$$\frac{\partial F}{\partial t} = k_{off}C - k^*_{on}F$$
$$\frac{\partial C}{\partial t} = k^*_{on}F - k_{off}C, \qquad \text{[S1]}$$

with $F + C = 1$. The parameter k^*_{on} is the product of the kinetic on rate and the average concentration of free binding sites. In steady state, the derivatives vanish and the bound and free fractions are given by

$$F_{eq} = \frac{k_{off}}{k^*_{on} + k_{off}}, \quad C_{eq} = \frac{k^*_{on}}{k^*_{on} + k_{off}}. \qquad \text{[S2]}$$

If a particle A is initially free at $t = 0$, the probability to find it in the free state after Δt is given by

$$F_A(\Delta t) = F_{eq}\left(1 + K^*_{eq}e^{-\left(k^*_{on}+k_{off}\right)\Delta t}\right). \qquad \text{[S3]}$$

Here, $K^*_{eq} = k^*_{on}/k_{off}$ is the pseudoequilibrium binding constant. In contrast, if a particle B is initially bound at $t = 0$, the probability to find it in the free state after Δt reads

$$F_B(\Delta t) = F_{eq}\left(1 - e^{-\left(k^*_{on}+k_{off}\right)\Delta t}\right). \qquad \text{[S4]}$$

The quantities $F_A(\Delta t)$ and $F_B(\Delta t)$ can also be regarded as the fraction of time that the particles have spent in the free state during Δt. Because complexes are assumed to be immobile, particles can only diffuse during their time in the free state. Thus, the apparent diffusion coefficient of the particles A and B is reduced because they are trapped part of the time. This apparent diffusion coefficient corresponds to the weighted average of the diffusion coefficients in the free state and the bound state, which, for a diffusion coefficient $D_{bound} \sim 0$ in the bound state, yields

$$D_A(\Delta t) = DF_A(\Delta t) = DF_{eq}\left(1 + K^*_{eq}e^{-\left(k^*_{on}+k_{off}\right)\Delta t}\right)$$
$$D_B(\Delta t) = DF_B(\Delta t) = DF_{eq}\left(1 - e^{-\left(k^*_{on}+k_{off}\right)\Delta t}\right). \qquad \text{[S5]}$$

For large times $\Delta t >> (k^*_{on} + k_{off})^{-1}$, both apparent diffusion coefficients converge to the effective diffusion coefficient $D_{eff} = DF_{eq} = D/(1 + K^*_{eq})$ (1). For small values of $\Delta t << (k^*_{on} + k_{off})^{-1}$, $D_A \to D$ and $D_B \to 0$, which reflect the initial conditions that particle A is free at $t = 0$ and particle B is bound at $t = 0$ (Fig. S1*B*). The average diffusion coefficient for the ensemble is the weighted average of the apparent diffusion coefficients D_A and D_B of the two pools (i.e., pool A with particles being initially free and pool B with particles being initially bound). Because the probability to find a free particle at $t = 0$ is F_{eq} and the probability to find a bound one is C_{eq}, the average diffusion coefficient is given by

$$\begin{aligned} D_{avg} &= F_{eq}D_A(\Delta t) + C_{eq}D_B(\Delta t) \\ &= F_{eq}DF_{eq}\left(1 + K^*_{eq}e^{-\left(k^*_{on}+k_{off}\right)\Delta t}\right) + C_{eq}DF_{eq}\left(1 - e^{-\left(k^*_{on}+k_{off}\right)\Delta t}\right) \\ &= DF_{eq}\left(F_{eq} + C_{eq}\right) = \frac{D}{1 + K^*_{eq}} = D_{eff}. \end{aligned} \qquad \text{[S6]}$$

As expected, the diffusion coefficient for the ensemble is not time-dependent and equals the effective diffusion coefficient. Thus, although the ensemble diffusion coefficient is D_{eff} on all time scales, the ensemble decomposes into a free pool and a bound pool on small time scales $\Delta t << (k^*_{on} + k_{off})^{-1}$, whereas the mobilities of the pools become similar for $\Delta t >> (k^*_{on} + k_{off})^{-1}$ (Fig. S1 *B* and *C*). In the first case, the size and the diffusion coefficient D of the free pool can be measured and the ratio of the rate constants $K^*_{eq} = k^*_{on}/k_{off}$ can be obtained from $F_{eq} = 1/(1 + K^*_{eq})$. This requires the accurate quantification of the free and immobile fractions. In the second case, only the effective diffusion coefficient D_{eff} can be determined. If the free diffusion coefficient is known, $K^*_{eq} = k^*_{on}/k_{off}$ can be calculated from the effective diffusion coefficient. In both scenarios, individual rate constants cannot be resolved because these can only be obtained from measurements on the intermediate time scale. In this regime, particles exchange between free pool and bound pool, and provide information about the binding reaction (Fig. S1*C*). Because conventional fluorescence recovery after photobleaching (FRAP) and fluorescence correlation spectroscopy (FCS) implementations are limited in their accessible time scales, only a distinct subset of kinetic rate constants can be determined that matches the relation $\Delta t \approx (k^*_{on} + k_{off})^{-1}$ (1, 2). In contrast, methods like raster image correlation spectroscopy, pair correlation analysis, or pixel-wise photobleaching evolution analysis (3PEA) include measurements on multiple scales, and thus cover a larger range of rates measurable for reaction-diffusion processes.

Derivation of the Theoretical 3PEA Framework for Free Diffusion. ***Bleaching a Point.*** In the following, an expression is derived that yields the probability for a particle to be bleached at pixel position $\vec{x}_0$ and to be subsequently detected via a decrease of the fluorescence signal when the focus is located at pixel position $\vec{x}_1$. The point spread functions (PSFs) are approximated by 3D-Gaussian geometry. This is sufficiently accurate for all experimentally relevant scenarios of this study because the 3PEA method relies on pixel distances rather than on the exact shape of the PSF. The equations derived here apply to normal diffusion. To account for other models or binding interactions, the diffusion propagator in the equations below is substituted with the corresponding expression. Thus, the theoretical description presented here can be used for any type of translocation process.

In the first step, we consider the probability P_{bleach} for a particle located at $\vec{x}$ to be bleached while the focus is located at $\vec{x}_0$. Assuming that bleaching is a first-order process with a bleach rate proportional to the illumination intensity, the amount

of fluorescent particles decreases with $\exp(-\gamma PSF^{1/2}\tau_{\text{bleach}}) \approx 1-\gamma PSF^{1/2}\tau_{\text{bleach}}$. Here, the PSF is defined according to Eq. **3** as the product of the illumination and detection PSF. Accordingly, the PSF for the bleaching process is given by

$$\begin{aligned} N^{\text{r2c}}_{\text{x}_0\to x_1}(\vec{x}_0,\vec{x}_1,\Delta t) &= \sum_i c\langle P_{\text{bleach},i}\rangle(\vec{x}_0) \int_{-\infty}^{\infty} dx' \int_{-\infty}^{\infty} dy' \int_{-\infty}^{\infty} dz'\ \Psi_{\text{det}}(\vec{x}',\vec{x}_1) \int_{x_i-r_x}^{x_i+r_x} dx \int_{y_i-r_y}^{y_i+r_y} dy \int_{z_i-r_z}^{z_i+r_z} dz\ P_{\text{diff}}(\vec{x},\vec{x}',\Delta t) \\ &= \sum_i \frac{cV_{\text{eff}}}{8}\langle P_{\text{bleach},i}\rangle(\vec{x}_0)\left[\text{erf}\left(\frac{x_i-x_1+r_x}{\sqrt{w_0^2/2+d^2}}\right)-\text{erf}\left(\frac{x_i-x_1-r_x}{\sqrt{w_0^2/2+d^2}}\right)\right] \\ &\quad\times\left[\text{erf}\left(\frac{y_i-y_1+r_y}{\sqrt{w_0^2/2+d^2}}\right)-\text{erf}\left(\frac{y_i-y_1-r_y}{\sqrt{w_0^2/2+d^2}}\right)\right]\left[\text{erf}\left(\frac{z_i-z_1+r_z}{\sqrt{z_0^2/2+d^2}}\right)-\text{erf}\left(\frac{z_i-z_1-r_z}{\sqrt{z_0^2/2+d^2}}\right)\right], \end{aligned} \quad \textbf{[S11]}$$

$PSF^{1/2}$. Because τ_{bleach} is the pixel time that is typically of the order of some microseconds, the latter approximation is appropriate, and the bleach probability can be expressed as

$$\begin{aligned} P_{\text{bleach}}(\vec{x},\vec{x}_0) &= \beta PSF^{1/2}(\vec{x},\vec{x}_0) \\ &= \beta\exp\left(-\frac{(x-x_0)^2+(y-y_0)^2}{w_{\text{b}}^2}-\frac{(z-z_0)^2}{z_{\text{b}}^2}\right). \end{aligned} \quad \textbf{[S7]}$$

In Eq. **S7**, $\beta=\gamma\tau_{\text{bleach}}\le 1$ is the bleach depth, and w_{b} and z_{b} denote the effective beam waist of the bleach PSF in lateral and axial directions, respectively. Because the high laser intensities during the bleach typically lead to an enlarged PSF, the specific set of structure parameters (w_{b}, z_{b}) is used to describe the bleach PSF.

In the second step, the probability P_{diff} for a particle located at $\vec{x}$ to diffuse to $\vec{x}'$ during time Δt is calculated. This probability is

$$P_{\text{diff}}(\vec{x},\vec{x}',\Delta t)=\frac{1}{(\pi d^2(\Delta t))^{3/2}}\exp\left(-\frac{(x-x')^2+(y-y')^2+(z-z')^2}{d^2(\Delta t)}\right). \quad \textbf{[S8]}$$

Here, D is the diffusion coefficient and $d^2(\Delta t)=4D\Delta t$ is the particle's mean squared displacement (MSD) for normal diffusion. Finally, the fluorescence intensity Ψ_{det} of a particle located at $\vec{x}'$ in the focus at $\vec{x}_1$ is calculated with Eq. **S9**:

$$\begin{aligned} \Psi_{\text{det}}(\vec{x}',\vec{x}_1) &= PSF(\vec{x}',\vec{x}_1) \\ &= \exp\left(-2\frac{(x'-x_1)^2+(y'-y_1)^2}{w_0^2}-2\frac{(z'-z_1)^2}{z_0^2}\right). \end{aligned} \quad \textbf{[S9]}$$

Based on Eqs. **S7**, **S8**, and **S9**, the fluorescence intensity reduction in $\vec{x}_1$ caused by particles bleached in $\vec{x}_0$ is proportional to

$$\begin{aligned} N^{\text{r2c}}_{\text{x}_0\to x_1}(\vec{x}_0,\vec{x}_1,\Delta t) &= c\int_{-\infty}^{\infty} dx' \int_{-\infty}^{\infty} dy' \int_{-\infty}^{\infty} dz'\ \Psi_{\text{det}}(\vec{x}',\vec{x}_1) \\ &\quad\times\int_{-\infty}^{\infty} dx \int_{-\infty}^{\infty} dy \int_{-\infty}^{\infty} dz\ P_{\text{bleach}}(\vec{x},\vec{x}_0)P_{\text{diff}}(\vec{x},\vec{x}',\Delta t). \end{aligned} \quad \textbf{[S10]}$$

Because overlapping bleach PSFs have to be considered for 2D bleach regions, the bleach PSF is split up into a sum of cuboids (Fig. S1). The intensity differences within a single cuboid are neglected, and the integral in Eq. **S10** is divided into two parts: the average cuboid bleach probability $\langle P_{\text{bleach},i}\rangle$ and the translocation probability $P^{\text{r2c}}_{x_i\to x_1}$:

with the average cuboid bleach probability $\langle P_{\text{bleach},i}\rangle(\vec{x}_0)=\frac{1}{V_{\text{b},i}}\int_{x_i-r_x}^{x_i+r_x}dx\int_{y_i-r_y}^{y_i+r_y}dy\int_{z_i-r_z}^{z_i+r_z}dz\ P_{\text{bleach}}(\vec{x},\vec{x}_0)$.

Each part of the sum in Eq. **S11** gives the reduced intensity due to the presence of particles bleached in a single cuboid centered at $\vec{x}_i$ with edge lengths $2r_x$, $2r_y$, and $2r_z$ and volume $V_{\text{b},i}$. For high laser intensities, which are typically used for FRAP experiments, the axial beam waist becomes very large. For this case (i.e., in the limit $z_{\text{b}}\to\infty, r_z\to\infty$), the axial dependence can be neglected and Eq. **S11** is written as

$$N^{\text{r2c}*}_{\text{x}_0\to x_1}(\vec{x}_0,\vec{x}_1,\Delta t)=cV_{\text{eff}}\sum_i\langle P_{\text{bleach},i}\rangle P^{\text{r2c}*}_{\text{x}_i\to x_1}(\vec{x}_i,\vec{x}_1,\Delta t), \quad \textbf{[S12]}$$

with

$$\begin{aligned} P^{\text{r2c}*}_{x_i\to x_1} &= \frac{1}{4}\left[\text{erf}\left(\frac{x_i-x_1+r_x}{\sqrt{w_0^2/2+d^2}}\right)-\text{erf}\left(\frac{x_i-x_1-r_x}{\sqrt{w_0^2/2+d^2}}\right)\right] \\ &\quad\times\left[\text{erf}\left(\frac{y_i-y_1+r_y}{\sqrt{w_0^2/2+d^2}}\right)-\text{erf}\left(\frac{y_i-y_1-r_y}{\sqrt{w_0^2/2+d^2}}\right)\right]. \end{aligned}$$

Bleaching a Line. For typical scan speeds, the line time τ_{l} is on the order of 1 ms. This corresponds to the dwell time of a freely mobile protein in one diffraction-limited spot. Therefore, diffusion during the bleach process of a single bleach line (or a line segment) can be simplified to reduce the computational cost of the calculations significantly. Based on the bleach probability in a single spot (Eqs. **S7**–**S12**), the bleach distribution after sequentially bleaching several spots along a line is derived. The intensity in $\vec{x}$ after n bleach events at positions $\vec{x}_i$ is given by

$$\begin{aligned} I(\vec{x},n) &= 1-P_{\text{bleach}}(\vec{x},n)=\prod_{i=0}^{n}\left(1-\beta\,PSF^{1/2}(\vec{x},\vec{x}_i)\right) \\ &= \exp\left(\ln\left(\prod_{i=0}^{n}\left(1-\beta\,PSF^{1/2}(\vec{x},\vec{x}_i)\right)\right)\right) \\ &= \exp\left(\sum_{i=0}^{n}\ln\left(1-\beta\exp\left(-\frac{(x-x_i)^2+(y-y_0)^2}{w_{\text{b}}^2}-\frac{(z-z_0)^2}{z_{\text{b}}^2}\right)\right)\right). \end{aligned} \quad \textbf{[S13]}$$

Thus, if a line between $-x_b$ and x_b is bleached, the intensity distribution can be expressed as

$$I(\vec{x}, \vec{x}_0, \vec{x}_b) = 1 - P_{\text{bleach}}(\vec{x}, \vec{x}_b) = \exp\left(\int_{-x_b}^{x_b} dx_i \mu \ln\left(1 - \beta \exp\left(-\frac{(x-x_i)^2+(y-y_0)^2}{w_b^2} - \frac{(z-z_0)^2}{z_b^2}\right)\right)\right), \quad \textbf{[S14]}$$

with an effective line bleach probability μ. To solve the integral given in Eq. **S14**, the logarithm is represented by a series expansion, yielding

$$\begin{aligned} P_{\text{bleach}}^{\text{line}}(\vec{x}, \vec{x}_0, \vec{x}_b) &= 1 - \exp\left(\int_{-x_b}^{x_b} dx_i \mu \sum_{n=1}^{\infty} \frac{(-1)^{n+1}}{n} \left(-\beta \exp\left(-\frac{(x-x_i)^2+(y-y_0)^2}{w_b^2} - \frac{(z-z_0)^2}{z_b^2}\right)\right)^n \right) \\ &= 1 - \exp\left(-\sum_{n=1}^{\infty} \frac{\mu}{n} \left(\beta \exp\left(-\frac{(y-y_0)^2}{w_b^2} - \frac{(z-z_0)^2}{z_b^2}\right)\right)^n \int_{-x_b}^{x_b} dx_i \exp\left(-n\frac{(x-x_i)^2}{w_b^2}\right)\right) \\ &= 1 - \exp\left(-\frac{\sqrt{\pi}}{2} \sum_{n=1}^{\infty} \frac{\mu w_n}{n} \left(\beta \exp\left(-\frac{(y-y_0)^2}{w_b^2} - \frac{(z-z_0)^2}{z_b^2}\right)\right)^n \left(\text{erf}\left(\frac{x+x_b}{w_n}\right) - \text{erf}\left(\frac{x-x_b}{w_n}\right)\right)\right), \end{aligned} \quad \textbf{[S15]}$$

with $w_n = \frac{w_b}{\sqrt{n}}$. The series in the exponential function decreases monotonically and the expression in the last line of Eq. **S15** converges. The series can be truncated as needed to compute the results numerically with the desired accuracy. For the calculations conducted here, the series was truncated at $n = 500$ and the bleach parameters $\beta = 0.2$ and $\mu = 2$ per pixel were used. In analogy to Eq. **S12**, the number of particles that translocate from a pixel $\vec{x}_0$ within the bleached line into pixel $\vec{x}_1$ can be calculated by replacing $P_{\text{bleach}}(\vec{x}, \vec{x}_0)$ with the line bleach probability $P_{\text{bleach}}^{\text{line}}(\vec{x}, \vec{x}_0)$ given in Eq. **S15**. The time stamp for each bleach event was assigned based on its x-position along the line. Thus, the sequential bleach events were correctly separated in time; however, their PSF was not assumed to be a Gaussian distribution but rather a slice of the line bleach PSF in Eq. **S15**. For pixels adjacent to the designated bleach spot that are bleached due to the spatial extension of the bleach PSF, the time stamp corresponding to the first/last point of the bleach region in the current scan line was assigned. This approach introduces errors in the bleach times that are on the order of the time the microscope's beam needs to translocate the distance that equals the lateral width of the bleach PSF, which is below 1 μm. For a scan speed of 1,400 Hz, a pixel time of roughly 0.4 μs, and a voxel size of 7.5 nm, this error is smaller than 50 μs.

Bleaching a 2D Region. In this section, the intensity distribution after bleaching a 2D region is derived. First, the fraction of particles bleached in a pixel of such a bleach region is calculated. This probability is not equal in all bleach pixels/lines. A particle can already be bleached when the focus is located at a precedent pixel/line due to the spatial extension of the bleach PSF and diffusive transport during the bleach process. The fraction of particles bleached in pixel $\vec{x}$ in the bleach region can be expressed with the recursive relation

$$N_{\text{bleach}}(\vec{x}, t) = P_{\text{bleach}}(\vec{x}, \vec{x}_0) \times \left(\langle N \rangle - \sum_{t_i < t} \sum_{\vec{x}' \in \text{PSF}_i} N_{\text{bleach}}(\vec{x}', t_i)\, P_{x' \to x}^{\text{r2r}}(\vec{x}', \vec{x}, t - t_i)\right). \quad \textbf{[S16]}$$

The probability $P_{x' \to x}^{\text{r2r}}(\vec{x}', \vec{x}, \Delta t)$ is the probability for a particle to be present in pixel $\vec{x}'$ and to translocate to pixel $\vec{x}$ during the time interval Δt. For cuboid voxels, this probability is given by

$$P_{x' \to x}^{\text{r2r}}(\vec{x}', \vec{x}, \Delta t) = \int_{x'-r_x}^{x'+r_x} d\tilde{x} \int_{y'-r_y}^{y'+r_y} d\tilde{y} \int_{z'-r_z}^{z'+r_z} d\tilde{z} \int_{x-r_x}^{x+r_x} d\hat{x} \int_{y-r_y}^{y+r_y} d\hat{y} \times \int_{z-r_z}^{z+r_z} d\hat{z}\; P_{\text{diff}}(\vec{\hat{x}}, \vec{\tilde{x}}, \Delta t) = \frac{1}{8} XYZ, \quad \textbf{[S17]}$$

with the following abbreviations:

$$\begin{aligned} X &= (\Delta x + 2r_x)\text{erf}\left(\frac{\Delta x + 2r_x}{d}\right) + (\Delta x - 2r_x)\text{erf}\left(\frac{\Delta x - 2r_x}{d}\right) \\ &\quad - 2\Delta x\, \text{erf}\left(\frac{\Delta x}{d}\right) + \sqrt{\frac{d^2}{\pi}}\left(e^{-\frac{(\Delta x+2r_x)^2}{d^2}} + e^{-\frac{(\Delta x-2r_x)^2}{d^2}} - 2e^{-\frac{\Delta x^2}{d^2}}\right) \\ Y &= (\Delta y + 2r_y)\text{erf}\left(\frac{\Delta y + 2r_y}{d}\right) + (\Delta y - 2r_y)\text{erf}\left(\frac{\Delta y - 2r_y}{d}\right) \\ &\quad - 2\Delta y\, \text{erf}\left(\frac{\Delta y}{d}\right) + \sqrt{\frac{d^2}{\pi}}\left(e^{-\frac{(\Delta y+2r_y)^2}{d^2}} + e^{-\frac{(\Delta y-2r_y)^2}{d^2}} - 2e^{-\frac{\Delta y^2}{d^2}}\right) \\ Z &= (\Delta z + 2r_z)\text{erf}\left(\frac{\Delta z + 2r_z}{d}\right) + (\Delta z - 2r_z)\text{erf}\left(\frac{\Delta z - 2r_z}{d}\right) \\ &\quad - 2\Delta z\, \text{erf}\left(\frac{\Delta z}{d}\right) + \sqrt{\frac{d^2}{\pi}}\left(e^{-\frac{(\Delta z+2r_z)^2}{d^2}} + e^{-\frac{(\Delta z-2r_z)^2}{d^2}} - 2e^{-\frac{\Delta z^2}{d^2}}\right) \end{aligned}$$

Here, d^2 is the particles' MSD and $\Delta x = \hat{x} - \tilde{x}$, $\Delta y = \hat{y} - \tilde{y}$, and $\Delta z = \hat{z} - \tilde{z}$. Based on Eqs. **S16** and **S17**, the intensity distribution after an arbitrary number of bleach events can be expressed according to

$$I(\vec{x}, t) = \varepsilon\left(\langle N \rangle - \sum_{t_i} \sum_{\vec{x}' \in \text{PSF}_i} N_{\text{bleach}}(\vec{x}', t_i)\, P_{x' \to x}^{\text{r2c}}(\vec{x}', \vec{x}, t - t_i)\right). \quad \textbf{[S18]}$$

3PEA for Reaction-Diffusion Processes. To apply 3PEA in the presence of reaction-diffusion processes, the propagator in Eq. **S8** is replaced with an expression that accounts for binding interactions. This reaction-diffusion propagator is derived in the following. The starting point is the dissociation of particles from a binding site, which is described by the differential equation

$$\frac{dN(t)}{dt} = -k_{\text{off}} N(t), \qquad \textbf{[S19]}$$

with the solution $N(t) = N_0\, e^{-k_{\text{off}} t}$. Thus, the probability for a bound particle to remain at the binding site for the time t_{res} is $P_{\text{b}}(t_{\text{res}}) = k_{\text{off}}\, e^{-k_{\text{off}} t_{\text{res}}}$, where the prefactor is required for normalization. The probability distribution for an arbitrary particle's residence time t_{res} in the presence of binding reactions with pseudoassociation rate k^*_{on} and dissociation rate k_{off} is

$$P_{\text{bound}}(t_{\text{res}}) = F_{\text{eq}}\delta(t_{\text{res}}) + C_{\text{eq}} k_{\text{off}} e^{-k_{\text{off}} t_{\text{res}}}. \qquad \textbf{[S20]}$$

Here, $F_{\text{eq}} = \frac{k_{\text{off}}}{k^*_{\text{on}}+k_{\text{off}}}$ and $C_{\text{eq}} = \frac{k^*_{\text{on}}}{k^*_{\text{on}}+k_{\text{off}}}$ are the free and bound fractions in steady state, respectively (see above). The first term is the probability to find a free particle, and the second term is the probability to find a particle bound for t_{res}. With this result, the propagator in Eq. **S8** can be redefined as

$$\begin{aligned} P_{\text{reac+diff}}(\vec{x}_0, \vec{x}_1, \Delta t) &= F_{\text{eq}} P_{\text{diff}}(\vec{x}_0, \vec{x}_1, \Delta t \cdot F_{\text{A}}(\Delta t)) \\ &+ C_{\text{eq}} \int_0^{\Delta t} dt_{\text{res}}\; k_{\text{off}} e^{-k_{\text{off}} t_{\text{res}}} P_{\text{diff}}(\vec{x}_0, \vec{x}_1, (\Delta t - t_{\text{res}}) \\ &\cdot F_{\text{A}}(\Delta t - t_{\text{res}})) + C_{\text{eq}} e^{-k_{\text{off}}\Delta t}\delta(\vec{x}_0 - \vec{x}_1). \qquad \textbf{[S21]} \end{aligned}$$

Here, $F_{\text{A}}(t)$ is the fraction of time a particle spends in the free state if it was free at $t = 0$ (derived above in Eq. **S3**). The first line of Eq. **S21** represents particles that are initially free and subsequently diffuse for $\Delta t \cdot F_{\text{A}}(\Delta t)$. The second line represents particles that are initially bound, dissociate after $t_{\text{res}} < \Delta t$, and diffuse for the rest of the time they spend in the free state [i.e., $(\Delta t - t_{\text{res}}) \cdot F_{\text{A}}(\Delta t - t_{\text{res}})$]. The third line represents particles that are initially bound and remain bound for $t_{\text{res}} > \Delta t$.

In general, the integral in the second line of Eq. **S21** has to be solved numerically. For special cases, an analytical reaction-diffusion propagator can be found. One case is binding that is much slower than the time scale of the measurement (i.e., $k_{\text{off}}^{-1} >> \Delta t$). Here, the probability to dissociate from a binding site within Δt can be neglected [i.e., $P_{\text{b}}(t_{\text{res}} < \Delta t) \to 0$] and the integrand in Eq. **S21** vanishes. The propagator converges to the sum of a diffusing pool and an immobile pool, with both having analytical propagators. For binding that occurs much faster than the time scale of the measurement (i.e., $k_{\text{off}}^{-1} << \Delta t$), the integrand in Eq. **S21** vanishes as well and one effectively diffusing pool with diffusion coefficient D_{eff} remains.

Convergence of 3PEA in the Limit of Infinitely Fast Scanning. In the limit of infinitely fast scanning and negligible beam waist, the above theoretical description yields the state-of-the-art FRAP model for a uniform disk derived previously (1, 3). For free diffusion, the probability to bleach a particle in $\vec{x}_0$ and to detect it in $\vec{x}_1$ (as fluorescence intensity decrease) is given by

$$P^{\text{lim}}_{\text{x}_0\to\text{x}_1}(\vec{x}_0, \vec{x}_1, \Delta t) = \frac{\beta}{4\pi D \Delta t} e^{-\frac{(x_1-x_0)^2+(y_1-y_0)^2}{4D\Delta t}}. \qquad \textbf{[S22]}$$

In case of infinitely fast scanning, the time Δt corresponds to the time τ_{f} to acquire one image frame. The number of bleached particles is equal in every pixel (i.e., Eq. **5** is not required). To obtain the intensity profile after having bleached a circle with radius R located around the center of the image (0, 0), the sum in Eq. **6** is replaced by an integral:

$$\begin{aligned} I(\vec{x}, m) &= \varepsilon \langle N \rangle \left(1 - \int_{\vec{x}' \in \text{ROI}} d\vec{x}'\; P^{\text{lim}}_{x'\to x}(\vec{x}', \vec{x}, m\tau_{\text{f}})\right) \\ &= \varepsilon \langle N \rangle \left(1 - \frac{\beta}{4\pi D m \tau_{\text{f}}} \int_0^R r r' dr' \int_0^{2\pi} d\phi'\, e^{-\frac{r^2+r'^2-2rr'\cos\phi'}{4Dm\tau_{\text{f}}}}\right) \\ &= \varepsilon \langle N \rangle \left(1 - \frac{\beta}{2Dm\tau_{\text{f}}} \int_0^R r r' e^{-\frac{r^2+r'^2}{4Dm\tau_{\text{f}}}} dr' I_0\left(\frac{rr'}{2Dm\tau_{\text{f}}}\right)\right). \end{aligned} \qquad \textbf{[S23]}$$

Here, $I_0(x)$ denotes the modified Bessel function of the first kind and m is the number of the postbleach frame. In the last step, the integral representation of $I_0(x)$ was used. The integral in the last line of Eq. **S23** corresponds to the one used by Soumpasis (equation 9 of ref. 3) to derive the well-known FRAP model for free diffusion; for $\beta = 1$, this is given by

$$\begin{aligned} I_{\text{ROI}}(m) &= \int_{\vec{x}\in\text{ROI}} d\vec{x}\, I(\vec{x}, m) \\ &= \varepsilon \langle N \rangle e^{-\frac{R^2}{2Dm\tau_{\text{f}}}} \left[I_0\left(\frac{R^2}{2Dm\tau_{\text{f}}}\right) + I_1\left(\frac{R^2}{2Dm\tau_{\text{f}}}\right)\right]. \end{aligned} \qquad \textbf{[S24]}$$

In analogy to the calculations above, the 3PEA limit for infinitely fast scanning and negligible beam waist in the presence of a reaction-diffusion process is derived as described below. Similar to Eq. **S22**, the probability to bleach a particle in $\vec{x}_0$ and to find it in $\vec{x}_1$ for the case of diffusion and binding (based on Eqs. **S20** and **S21**) amounts to

$$\begin{aligned} P^{\text{lim}}_{\text{b,x}_0\to\text{x}_1}(\vec{x}_0, \vec{x}_1, \Delta t) &= \left(P_{\text{bound}} \otimes P^{\text{lim}}_{\text{x}_0\to\text{x}_1}\right)(\vec{x}_0, \vec{x}_1, \Delta t) \\ &+ C_{\text{eq}} e^{-k_{\text{off}}\Delta t}\delta(\vec{x}_0, \vec{x}_1). \end{aligned} \qquad \textbf{[S25]}$$

Here, $\otimes$ is the convolution operator. In the limit of vanishing beam waist, the Dirac delta distribution is obtained; the bleach depth was set to $\beta = 1$. The relation between the integrated intensity in the bleach region of interest and the transition probability in Eq. **S25** is given by

$$\begin{aligned} I_{\text{ROI}}(m) &= \int_{\vec{x}\in\text{ROI}} I(\vec{x}, m) \\ &= \varepsilon \langle N \rangle \left(1 - \int_{\vec{x}\in\text{ROI}} d\vec{x} \int_{\vec{x}\in\text{ROI}} d\vec{x}'\; P^{\text{lim}}_{\text{b},x'\to x}(\vec{x}', \vec{x}, m\tau_{\text{f}})\right) \\ &= \varepsilon \langle N \rangle \left(1 - \int_{\vec{x}\in\text{ROI}} d\vec{x} \int_{\vec{x}'\in\text{ROI}} d\vec{x}'\; \left(P_{\text{bound}} \otimes P^{\text{lim}}_{\text{x}'\to\text{x}}\right)\right. \\ &\left.(\vec{x}', \vec{x}, m\tau_{\text{f}}) - C_{\text{eq}} e^{-k_{\text{off}} m\tau_{\text{f}}}\right). \end{aligned} \qquad \textbf{[S26]}$$

Because the convolution in Eq. **S26** cannot be calculated analytically, an expression for the Laplace-transformed intensity is derived. Starting from the Laplace transform for the pure dif-

fusion case (1), together with the results from the previous section, the following relation is obtained:

$$\bar{I}_{\mathrm{ROI}}(p) = \varepsilon\langle N\rangle L\left\{1 - \int_{\vec{x}\in\mathrm{ROI}} d\vec{x} \int_{\vec{x}'\in\mathrm{ROI}} d\vec{x}'\, P^{\lim}_{x'\to x}\left(\vec{x}', \vec{x}, t\right)\right\}$$
$$= \varepsilon\langle N\rangle\left(\frac{1}{p} - \frac{1}{p}\left(1 - 2K_1\left(R\sqrt{\frac{p}{D}}\right) I_1\left(R\sqrt{\frac{p}{D}}\right)\right)\right). \quad \textbf{[S27]}$$

Here, $L\{f(t)\}$ denotes the Laplace transform. Thus, for the case of binding and diffusion, Eq. **S27** reads

$$\bar{I}_{\mathrm{ROI}}(p) = \varepsilon\langle N\rangle\left(\frac{1}{p} - L\left\{\int_{\vec{x}\in\mathrm{ROI}} d\vec{x} \int_{\vec{x}'\in\mathrm{ROI}} d\vec{x}' \right.\right.$$
$$\left.\left.(P_{\mathrm{bound}} \otimes P^{\lim}_{x'\to x})\left(\vec{x}', \vec{x}, t\right) + C_{\mathrm{eq}} e^{-k_{\mathrm{off}} t}\right\}\right)$$
$$= \varepsilon\langle N\rangle\left(\frac{1}{p} - L\{P_{\mathrm{bound}}(t)\} \int_{\vec{x}\in\mathrm{ROI}} d\vec{x} \int_{\vec{x}'\in\mathrm{ROI}} d\vec{x}' \right.$$
$$\left. L\left\{P^{\lim}_{x'\to x}\left(\vec{x}', \vec{x}, t'\right)\right\} - C_{\mathrm{eq}} L\left\{e^{-k_{\mathrm{off}} t}\right\}\right)$$
$$= \varepsilon\langle N\rangle\left(\frac{1}{p} - \frac{1}{p} L\{P_{\mathrm{bound}}(t)\}\left(1 - 2K_1\left(\sqrt{p'}\right) I_1\left(\sqrt{p'}\right)\right) - \frac{C_{\mathrm{eq}}}{p + k_{\mathrm{off}}}\right). \quad \textbf{[S28]}$$

In the first step, the convolution theorem for Laplace transforms was used. Furthermore, the dimensionless variable $t' = t\frac{D_{\mathrm{A}}(t)}{R^2}$ with its Laplace variable $p' = p\frac{R^2}{\bar{D}(p)} = \frac{R^2}{L\{D_{\mathrm{A}}(t)\}}$ was introduced. The solution for $L\{P_{\mathrm{bound}}(t)\}$ with $P_{\mathrm{bound}}(t)$ as defined in Eq. **S20** is

$$L\{P_{\mathrm{bound}}(t)\} = F_{\mathrm{eq}} L\{\delta(t)\} + C_{\mathrm{eq}} k_{\mathrm{off}} L\left\{e^{-k_{\mathrm{off}} t_{\mathrm{res}}}\right\}$$
$$= \left(F_{\mathrm{eq}} + C_{\mathrm{eq}} \frac{k_{\mathrm{off}}}{p + k_{\mathrm{off}}}\right) = F_{\mathrm{eq}}\left(1 + \frac{k^*_{\mathrm{on}}}{p + k_{\mathrm{off}}}\right). \quad \textbf{[S29]}$$

Based on Eqs. **S28** and **S29**, the expression for the Laplace-transformed intensity in the bleach spot can be written as

$$\bar{I}_{\mathrm{ROI}}(p) = \varepsilon\langle N\rangle\left(\frac{1}{p} - \frac{1}{p} F_{\mathrm{eq}}\left(1 + \frac{k^*_{\mathrm{on}}}{p + k_{\mathrm{off}}}\right)\left(1 - 2K_1\left(\sqrt{p'}\right) I_1\left(\sqrt{p'}\right)\right) - \frac{C_{\mathrm{eq}}}{p + k_{\mathrm{off}}}\right), \quad \textbf{[S30]}$$

with $p' = p\frac{R^2}{\bar{D}(p)} = \frac{pR^2}{D}\left(1 + \frac{k^*_{\mathrm{on}}}{p + k_{\mathrm{off}}}\right)$.

This is the result obtained previously for reaction-diffusion processes by Sprague et al. (1).

Calculating Effective Translocation Probability Distributions. Based on the microscope's scan parameters, the characteristic spatial and temporal distance to a set of bleach events can be calculated for every pixel of the image. The characteristic temporal distance was determined according to

$$\overline{\Delta t} = \frac{\sum_{\vec{x}\in\mathrm{ROI}} \sum_{\vec{x}'\in\mathrm{PSF}} \Delta t\left(\vec{x}, \vec{x}'\right) \cdot |\vec{x} - \vec{x}'|^{-1}}{\sum_{\vec{x}\in\mathrm{ROI}} \sum_{\vec{x}'\in\mathrm{PSF}} |\vec{x} - \vec{x}'|^{-1}}. \quad \textbf{[S31]}$$

Here, $\Delta t(\vec{x}, \vec{x}')$ represents the temporal distance between pixels $\vec{x}$ and $\vec{x}'$ (according to Eq. **1**). The $|\vec{x}–\vec{x}'|^{-1}$ term is a weight factor accounting for the fact that particles diffusing larger distances are underrepresented in a given pixel, because in a 2D process, every pixel $\vec{x}'$ can be regarded as a radial line segment of a circle around the originating pixel $\vec{x}$. For simplicity, it was neglected that bleaching also occurs at pixels outside the nominal bleach region due to the spatial extension of the PSF. The characteristic spatial distance was calculated in an analogous manner:

$$\overline{\Delta x} = \frac{\sum_{\vec{x}\in\mathrm{ROI}} \sum_{\vec{x}'\in\mathrm{PSF}} \Delta x\left(\vec{x}, \vec{x}'\right) \cdot |\vec{x} - \vec{x}'|^{-1}}{\sum_{\vec{x}\in\mathrm{ROI}} \sum_{\vec{x}'\in\mathrm{PSF}} |\vec{x} - \vec{x}'|^{-1}}. \quad \textbf{[S32]}$$

Similar to Eq. **S31**, $\Delta x(\vec{x}, \vec{x}') = |\vec{x} - \vec{x}'|$ represents the spatial distance between pixels $\vec{x}$ and $\vec{x}'$. Based on the assignment of Δx and Δt, translocation probabilities can be estimated from the pixel intensities as explained in the main text.

3PEA Implementation. The workflow for the 3PEA data analysis of protein mobility in the presence of interactions with immobile obstacles, such as chromatin, is illustrated in Fig. S7. The experimental bleach profile is fitted with the diffusion library to determine the apparent diffusion coefficient D. The value of D retrieved from the diffusion fit is compared with the free diffusion coefficient D_{free} that can be derived by different approaches: (*i*) The protein mobility in the cytosol can be measured, which yields D in the absence of chromatin interactions; (*ii*) a similar-sized inert protein can be measured, such as, for example, the green autofluorescent protein (GFP) pentamer used here; and (*iii*) the diffusion coefficient can be calculated based on its molecular weight and/or structure (4). A value of the apparent diffusion coefficient D similar to D_{free} indicates that binding interactions can be neglected. If D is significantly smaller than D_{free}, it is likely that binding reactions decrease protein mobility. Other reasons for a reduced diffusion coefficient include caging effects or the formation of a multimeric protein complex that displays an increased molecular weight M over that of the monomeric protein, with D being proportional to $M^{-1/3}$ for a spherical protein. However, these contributions typically lead to only moderate changes. Protein complexes with M as high as 1–2 MDa appear to be unrestricted in terms of the accessible nuclear space (5), and up to a GFP pentamer, protein mobilities were found to be very similar in the cytoplasm and in the nucleoplasm (6). In the case of protein binding, the interaction with chromatin is described by a pseudoequilibrium constant $K^*_{\mathrm{eq}} = k^*_{\mathrm{on}}/k_{\mathrm{off}}$, with k^*_{on} also including the concentration of binding sites according to the formalism outlined above. To separate the diffusion of the protein from the binding contribution, the bleach profile is fitted to a reaction-diffusion model. If both the diffusion and the reaction-diffusion fits are of similar quality, a transient binding interaction is present that is included in the value of the effective diffusion coefficient. Otherwise, the fit to the full reaction-diffusion library retrieves k^*_{on} and k_{off}. For very large dissociation rates, only a lower limit can be calculated, which is determined by the time resolution of 3PEA. In the current implementation, it is limited by the error of the bleach time assignment, which is roughly 50 μs. Thus, dissociation rates up to about 10,000 s^{-1} can be resolved.

1. Sprague BL, Pego RL, Stavreva DA, McNally JG (2004) Analysis of binding reactions by fluorescence recovery after photobleaching. *Biophys J* 86(6):3473–3495.
2. Michelman-Ribeiro A, et al. (2009) Direct measurement of association and dissociation rates of DNA binding in live cells by fluorescence correlation spectroscopy. *Biophys J* 97 (1):337–346.
3. Soumpasis DM (1983) Theoretical analysis of fluorescence photobleaching recovery experiments. *Biophys J* 41(1):95–97.
4. Ortega A, Amorós D, García de la Torre J (2011) Global fit and structure optimization of flexible and rigid macromolecules and nanoparticles from analytical ultracentrifugation and other dilute solution properties. *Methods* 54(1):115–123.
5. Görisch SM, Wachsmuth M, Tóth KF, Lichter P, Rippe K (2005) Histone acetylation increases chromatin accessibility. *J Cell Sci* 118(Pt 24):5825–5834.
6. Pack C, Saito K, Tamura M, Kinjo M (2006) Microenvironment and effect of energy depletion in the nucleus analyzed by mobility of multiple oligomeric EGFPs. *Biophys J* 91(10):3921–3936.

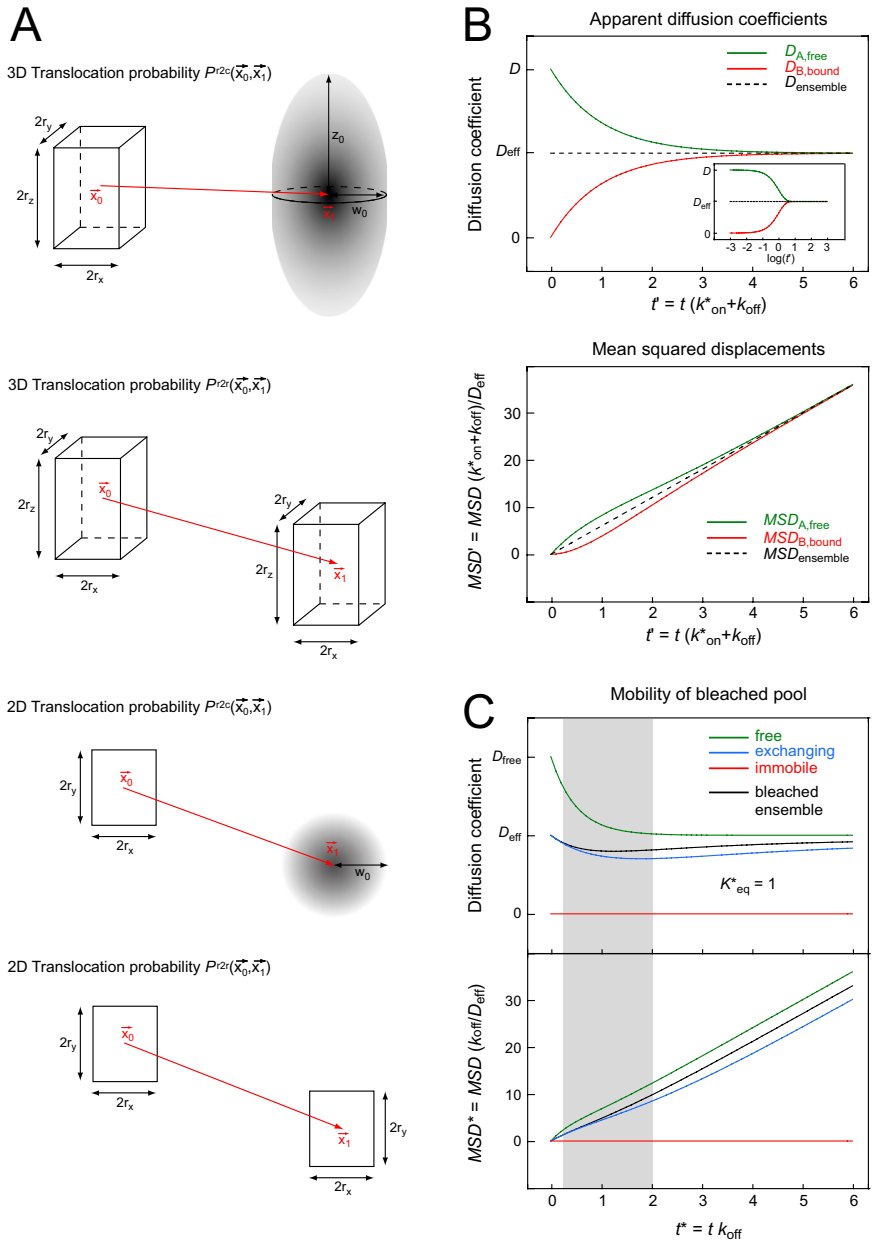

Fig. S1. Function definitions and behavior of reaction-diffusion processes. (*A*) Translocation probabilities used for the derivation of the theoretical 3PEA framework are visualized. P^{r2r} is the translocation probability between two cubes or rectangles, P^{r2c} is the translocation probability between a cube and a 3D-Gaussian distribution or a rectangle and a 2D-Gaussian distribution. (*B*) The scale-dependent behavior of reaction-diffusion processes is illustrated, and the time-dependent apparent diffusion coefficients for the particles that are initially free or bound are shown. (*C*) The bound pool can be further subdivided into an immobile pool (bound longer than t^*) and an exchanging pool (bound shorter than t^*) according to the propagator in Eq. **8**. On different scales, different pools are present, allowing for retrieval of distinct observables. For very short measurement scales, only an immobile fraction and a mobile fraction diffusing with D are present; for very large measurement scales, only one pool diffusing with D_{eff} is present. In both cases, the individual rate constants are not obtained. Rather, measurements on the intermediate time scale have to be conducted to characterize the process fully.

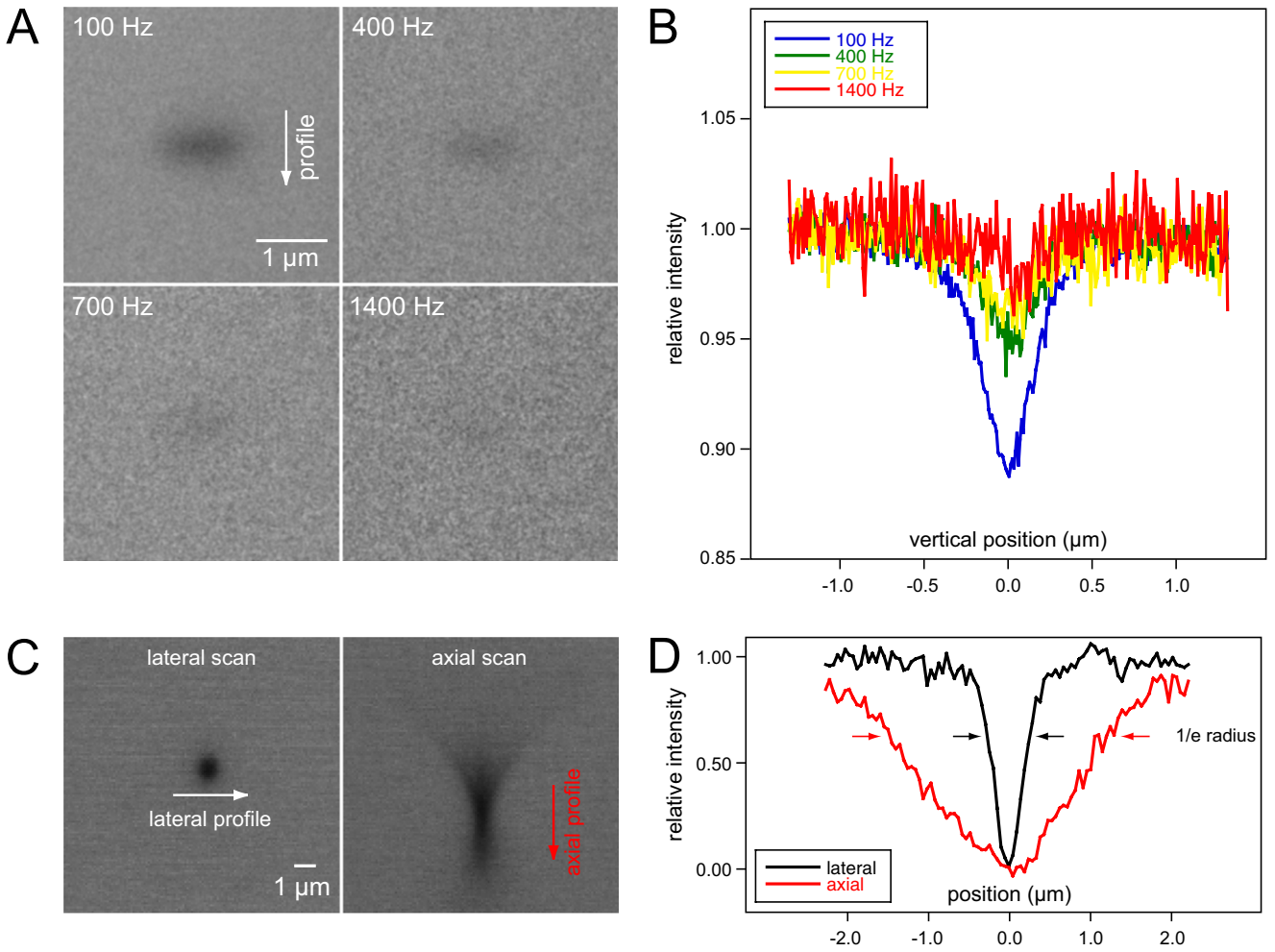

Fig. S2. Calibration of the bleach PSF. The bleach PSF in lateral and axial direction was determined with a GFP solution dried on a coverslip and a fluorescent plastic slide (Chroma Technology Corp.), respectively. (*A*) Line segments were bleached with different scan speeds to obtain the lateral geometry of the bleach PSF from the dried GFP sample. (*B*) Intensity perpendicular to the bleached line segments from *A* was plotted to determine the effective bleach depth. (*C*) A spot was bleached on the chroma slide to determine the axial geometry of the bleach PSF. (*D*) Intensity profiles from *C* were plotted to estimate the beam waist for the bleach PSF.

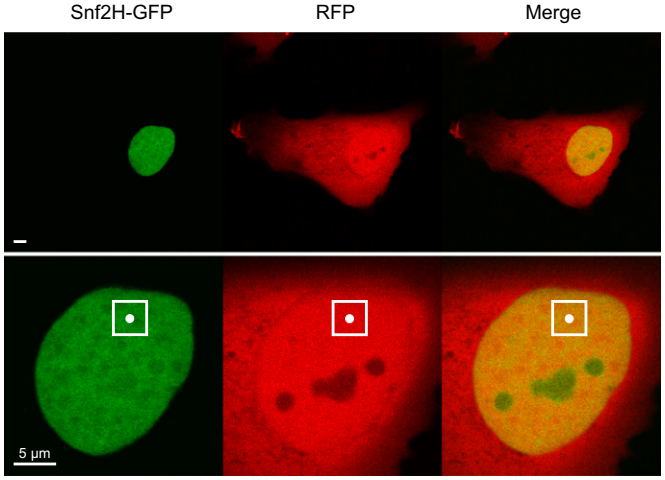

Fig. S3. Representative cell coexpressing Snf2H-GFP and red fluorescent protein (RFP). U2OS cells stably expressing Snf2H-GFP were transiently transfected with a plasmid coding for TagRFP. The bleach region was positioned in a region of the nucleoplasm where both proteins were mostly homogeneously distributed.

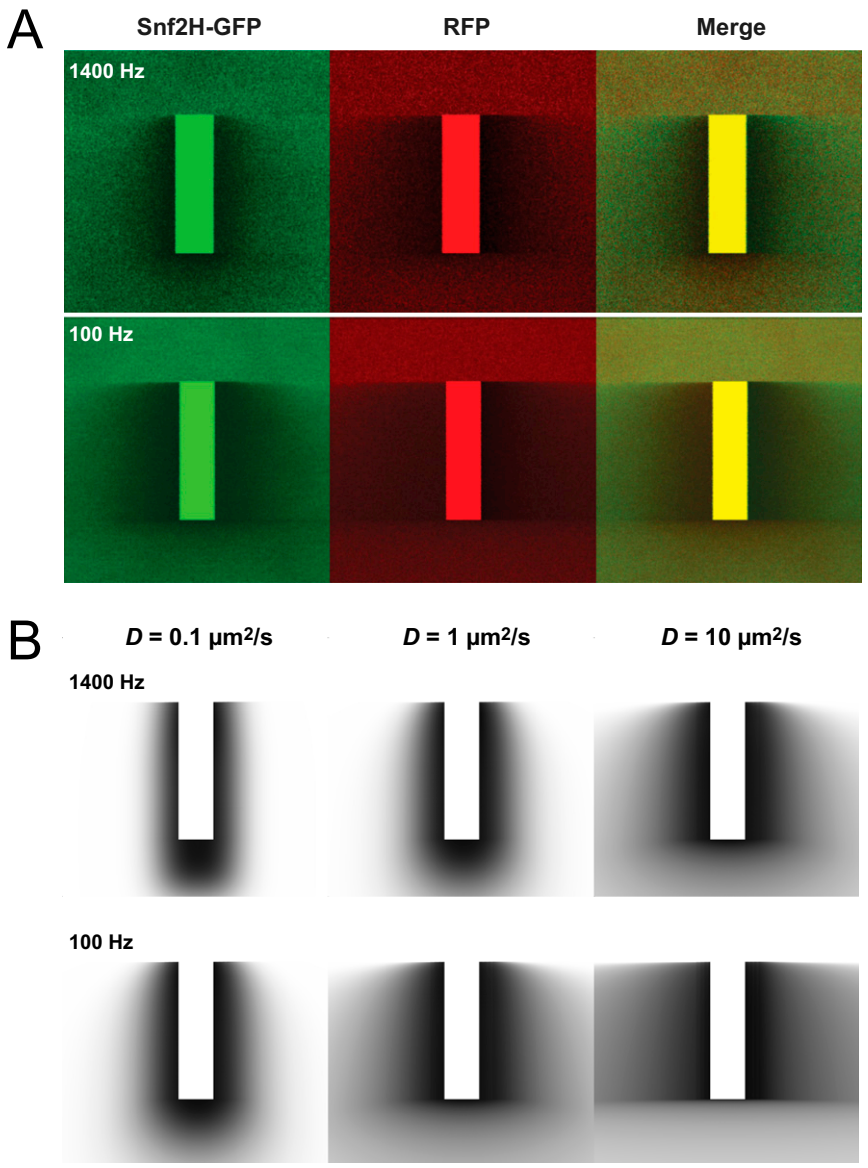

Fig. S4. Experimental implementation of 3PEA for a rectangular bleach region. (*A*) A stable Snf2H-GFP U2OS cell line was transfected with free red fluorescent protein (RFP) (Fig. S3), and the mobilities of both proteins were measured in a 3PEA experiment. Scan speeds of 100 Hz and 1,400 Hz were used for raster acquisition and bleaching. The rectangular bleach regions had dimensions of 2 μm × 0.5 μm (experiments with a circular bleach geometry are shown in Fig. 2). As expected, the bleach coronas became broader for increasing diffusion coefficients and decreasing scan speeds. In the merge images, the less mobile protein can be readily identified by visual inspection of the predominant color in the area adjacent to the bleach region (here, Snf2H-GFP in green). (*B*) Exemplary theoretical bleach profiles for different diffusion coefficients calculated for the parameters used in the experiments, with 512 × 512 pixels and 7.5-nm voxel size. The experimental Snf2H-GFP profile seems to be most similar to the $D = 1\ \mu m^2 \cdot s^{-1}$ case, whereas the RFP profile is better approximated with $D = 10\ \mu m^2 \cdot s^{-1}$.

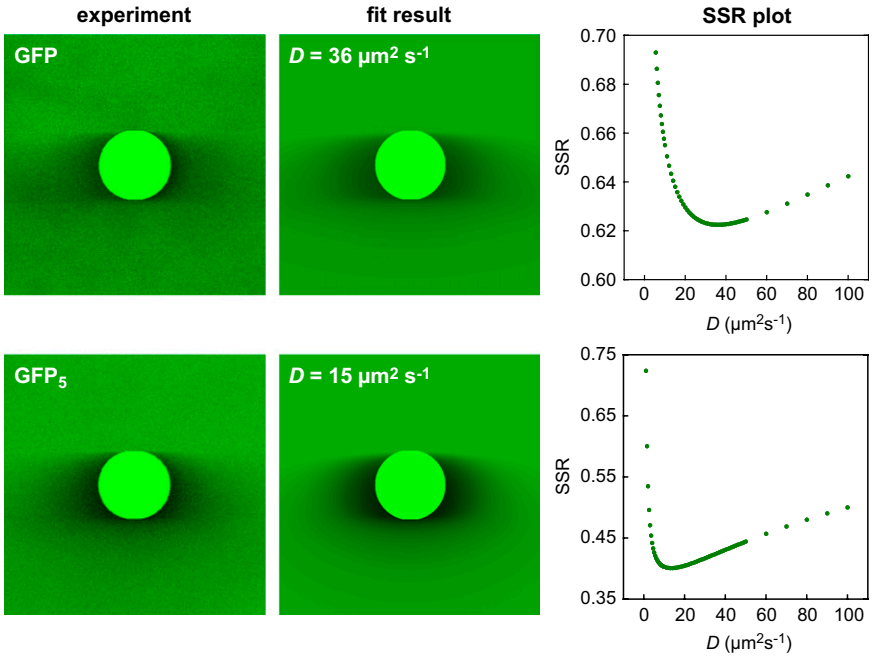

Fig. S5. Diffusion coefficient of free GFP and a GFP pentamer (GFP_5) measured by 3PEA in the nucleus. U2OS cells stably expressing free GFP or GFP_5 were subjected to 3PEA. Diffusion coefficients of $D = 36 \pm 5$ $\mu m^2 \cdot s^{-1}$ and $D = 15 \pm 2$ $\mu m^2 \cdot s^{-1}$ were determined for GFP and GFP_5, respectively. The experimental fluorescence intensity profile, the corresponding image for the best fit, and the sum of squared residuals (SSR) plot are shown.

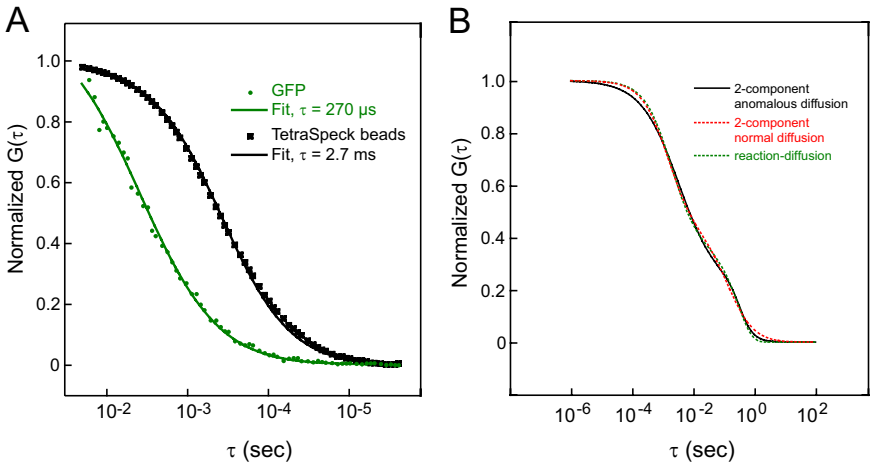

Fig. S6. Experimental calibration of fluorescence correlation spectroscopy (FCS) measurements and comparison of different FCS fit models. (*A*) Diffusion times of GFP and TetraSpeck 100 beads. The dwell time of free GFP expressed in U2OS cells was measured by FCS. As a reference, TetraSpeck beads with a diameter of 100 nm and a known diffusion coefficient of $D = 4.4$ $\mu m^2 \cdot s^{-1}$ were measured in aqueous solution. From the dwell time difference, an effective diffusion coefficient of $D = 44$ $\mu m^2 \cdot s^{-1}$ was determined for GFP. (*B*) FCS autocorrelation curves for reaction-diffusion processes (green) have a very similar shape as autocorrelation curves with two diffusive components (red). Thus, it is difficult to decide if the second component originates from jiggling of the chromatin fiber or from a reaction-diffusion process with an immobile substrate. For comparison, the best fit of a two-component anomalous diffusion model to an experimental curve for Snf2H-GFP is shown (black). Curves were plotted according to the equations in the studies by Michelman-Ribeiro et al. (1) and Erdel et al. (2) with the parameters for two-component anomalous diffusion ($D_{fast} = 6$ $\mu m^2 \cdot s^{-1}$, $D_{slow} = 0.06$ $\mu m^2 \cdot s^{-1}$, $\alpha_{fast} = 0.7$, $\alpha_{slow} = 2.0$, $f_{fast} = 0.78$), two-component normal diffusion ($D_{fast} = 15$ $\mu m^2 \cdot s^{-1}$, $D_{slow} = 0.16$ $\mu m^2 \cdot s^{-1}$, $f_{fast} = 0.57$), and reaction-diffusion ($K^*_{eq} = 0.59$, $k_{off} = 3.2$ s^{-1}, $D = 12$ $\mu m^2 \cdot s^{-1}$).

1. Michelman-Ribeiro A, et al. (2009) Direct measurement of association and dissociation rates of DNA binding in live cells by fluorescence correlation spectroscopy. *Biophys J* 97(1): 337–346.
2. Erdel F, Schubert T, Marth C, Längst G, Rippe K (2010) Human ISWI chromatin-remodeling complexes sample nucleosomes via transient binding reactions and become immobilized at active sites. *Proc Natl Acad Sci USA* 107(46):19873–19878.

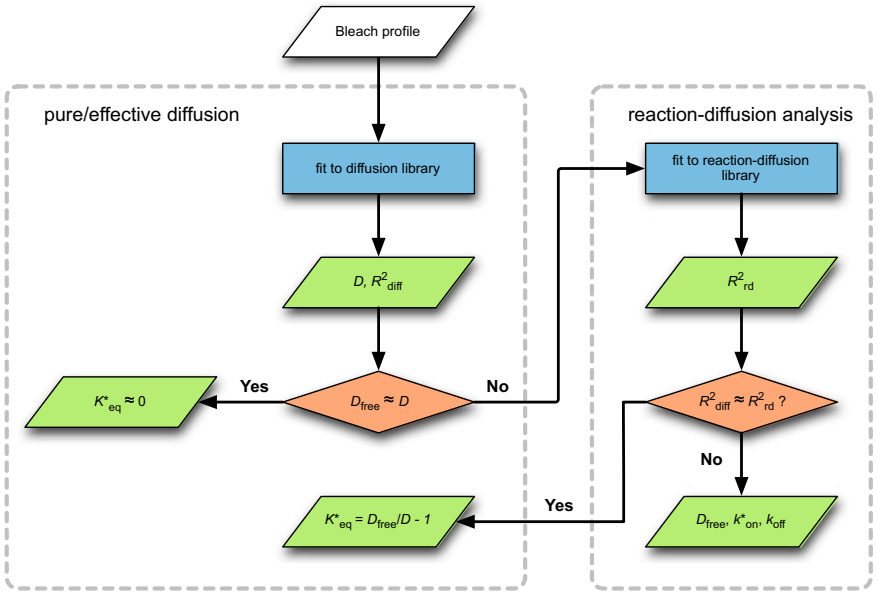

Fig. S7. Workflow for 3PEA. The general workflow for the mobility analysis of different proteins by 3PEA is shown. Based on this methodology, the effective diffusion coefficient for the proteins can be determined. Furthermore, the binding interactions between the protein and immobile obstacles can be characterized as described in the main text and *SI Text*.

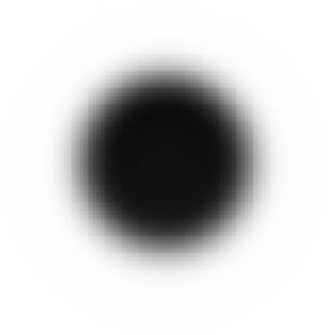

Movie S1. Simulated bleach experiment with $D = 1\ \mu m^2 \cdot s^{-1}$. Confocal light scanning microscopes acquire and bleach images via a raster scan process. Pixels are sequentially illuminated from the upper left pixel to the lower right pixel. In the standard unidirectional mode, all lines are scanned from left to right. Thus, after a line has been scanned, the microscope's illumination beam moves to the left pixel of the next line ("fly-back"). (*Left*) Current beam position is depicted. During fly-back, a gray strip appears in the lower left corner. The bleach region consists of one pixel located in the center of the image. When the illumination beam reaches this pixel, the intensity increases and a Gaussian-shaped profile is bleached into the pool of fluorescent particles. (*Center*) Current intensity distribution that could be observed by looking at all particles simultaneously is depicted (fluorescent particles are represented in white, bleached particles are represented in black). The intensity distribution does not correspond to the acquired image, because the microscope detects only one pixel at a time at the point where the illumination beam is located (*Left*), which leads to the CLSM image (*Right*). The bleach profile is asymmetrical, because the pixels above the bleach region are acquired before bleaching has occurred and because diffusion takes place during the acquisition process. For the simulation, a voxel size of 100 nm, a pixel dwell time of 5 μs, and a diffusion coefficient of $1\ \mu m^2 \cdot s^{-1}$ were used.

Movie S1

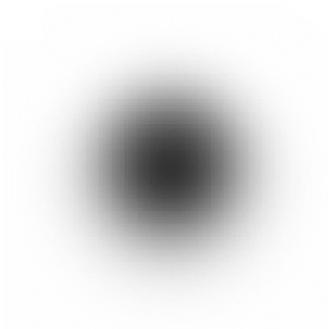

Movie S2. Simulated bleach experiment with $D = 10\ \mu m^2 \cdot s^{-1}$. The bleach experiment is the same as in Movie S1 but with a diffusion coefficient of $10\ \mu m^2 \cdot s^{-1}$. Diffusion during the bleach process is evident, leading to a bleach profile that is broadened in its lower part.

Movie S2

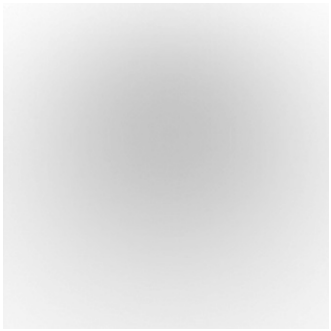

Movie S3. Simulated bleach experiment with $D = 100\ \mu m^2 \cdot s^{-1}$. The bleach experiment is the same as in Movie S1 but with a diffusion coefficient of $100\ \mu m^2 \cdot s^{-1}$. Here, diffusion occurring during the bleach process is significant. The bleach profile becomes very broad at its lower part, and the remaining bleach depth after completion of the image frame is very small. Thus, the signal would be insufficient for a conventional FRAP analysis.

Movie S3